Carpathian Journal of Earth and Environmental Sciences, August 2019, Vol. 14, No. 2, p. 473 - 482; DOI:10.26471/cjees/2019/014/096

THE SMALL-SCALE TECTONIC LANDFORMS OF GYIRONG WATERSHED IN THE MIDDLE HIMALAYAN OROGEN, TIBET, CHINA

Lu CHEN[1, 3], Aike KAN[*2, 3] & Yingjie WANG[3]

[1]Institute of Humanity Resources in Western China, Chengdu Normal College, Chengdu 611130, China, 051052@cdnu.edu.cn

[2]College of Geophysics, Chengdu University of Technology, Chengdu 610059, China, kanaike@qq.com

[3]State Key Laboratory of Resource and Environmental Information System, Institute of Geographic Sciences and Natural Resources Research, Chinese Academy of Sciences, Beijing 100101, China, wangyj@igsnrr.ac.cn

Abstract: The relationship between small-scale topographic features and tectonic response of orogenic belts is often neglected due to scale differences in topographic data. Using Aster GDEM2, we calculated swath elevation, 200m topographic relief, and average slope angle of a small-scale watershed in the middle Himalayan orogen. Based on the geological history of Gyirong and data on the Himalayan uplift process, this study analyzed the topographic characteristics of Gyirong watershed, discussed the relationships between landform and structure, lithology, and climate, and compared slope stability. The results showed that the topographic elevation characteristics retained correspondence to local basement forms and tectonic associations. Periodic spatial change at the summit level had a clear response to the structural distribution, and may support the theory that the Gyirong basin floor is a combination of normal and reverse faults. Average height increased at first and then stabilized, and these morphological characteristics and distribution patterns provide topographic evidence for the interpretation of tectonic uplift and erosional accumulation, which confirmed that 4000m was the vertical differentiation boundary for the tectonic landform. Although climate, landforms, tectonics, and lithology vary across different orogenic belts, the similar slope angle threshold provided the insight that erosion is the tectonic genesis to equilibrium of heterogeneous hillsides at different scales.

Keywords: tectonic landform; digital topographic analysis; Aster GDEM2; the Middle Himalayan orogen; Gyirong watershed

1. INTRODUCTION

Studies of orogen terrain features explore the tectonic and erosion processes to obtain an understanding of the geomorphic patterns and orogenic development. Digital elevation models (DEM) provide elevation data at various scales and in a uniform format (Burbank, 1992), while digital terrain analysis quantitatively calculates terrain features. Considering the large spatial scale and complicated surface processes of orogens, there are natural advantages to applying DEM, which when combined with traditional analyses of tectonic movement, stratigraphic lithology, and erosion, has become an important way to interpret geomorphologic pattern and process (Vijith et al., 2017; Dong et al., 2018; Petrik & Jordan, 2017).

"Digital" studies with derived indices from a DEM have significant advantages (Artugyan & Urdea, 2016), but problems remain related to the following aspects: First, the analytical capabilities of terrain indices for true surfaces vary across different regions. Different DEMs also have different qualities, and even for the same terrain index there may still be deviations in sampling attribute values (Gonga-Saholiariliva et al., 2013). Existing studies have lacked information about the suitability of DEM data with respect to geomorphological objects. Research has also used quantitative topographic analysis to define the mechanisms of development, which is not sufficient. In orogenic belts, geological background studies over large time-space scales are relatively advanced, but over a relatively recent geological period, such as neotectonic movement, the relationships between structure, lithology, climate, and geomorphology remain to be explored.

Consequently, frequency-magnitude relationships, scale effects, critical phenomena, and complicated responses of geomorphological processes still pose important theoretical problems for geomorphological studies (Xu et al., 2009).

This study attempts to establish the basic genesis analysis pattern of orogenic tectonic landforms. By calculating three digital indices (i.e., elevation attributes, local relief, and slope), this paper quantifies the terrain features of a small-scale watershed in the middle Himalayan orogen. Based on regional geological history and data on the Himalayan uplift process, tectonic landform responses to structure, lithology, and climate are discussed.

2. STUDY AREA

2.1 Study area overview

The following basic conclusions have been drawn about the geological setting and evolution of Himalayan orogen (Molnar & Tapponnier, 1975; Yin, 2006; Le Fort, 1996): During the early and late Miocene (10-20Ma), the Indo-European continent experienced intense collision orogeny with large-scale thrusts and north-south extensional detachments that generated a series of imbricate structures with north-dipping sections.

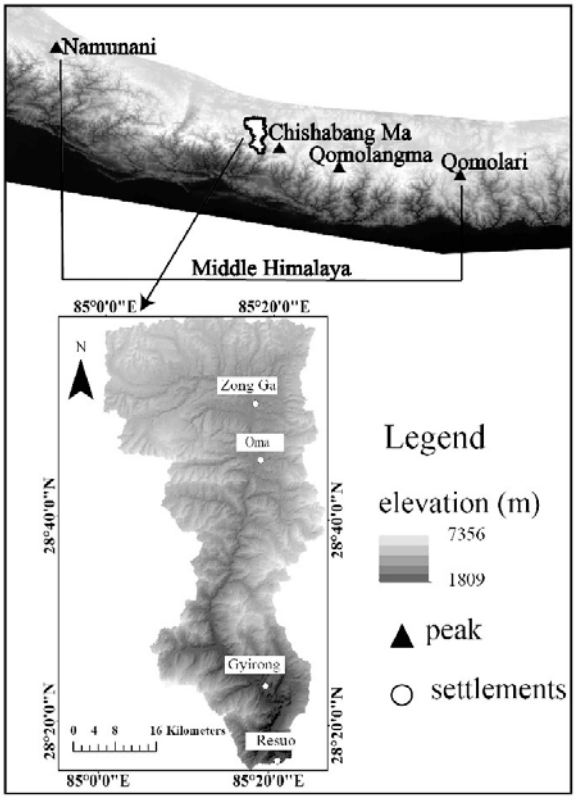

Figure 1. location map of Gyirong watershed

The Gyirong watershed is a developed valley located in the north of the middle Himalayan orogen(Fig. 1). Marine and plateau continental climate features are joined in the hinterland, producing five climate belts and six vertical soil and vegetation zones within an elevation range of 5 500m (Chen et al., 2011). It occupies an area of 2 108.59km^2 between 85°10′-85°40′E and 28°15′-28°45′N.

2.2. Geological setting

Wang (2008) analyzed the distribution sequence in Gyirong tectonic basin, subdividing it into the Mala Dome, Gyirong Depression, Gyirong-Oma Depression, Oma Depression, and Southern Oma Small Depression (Fig. 2, A-E).

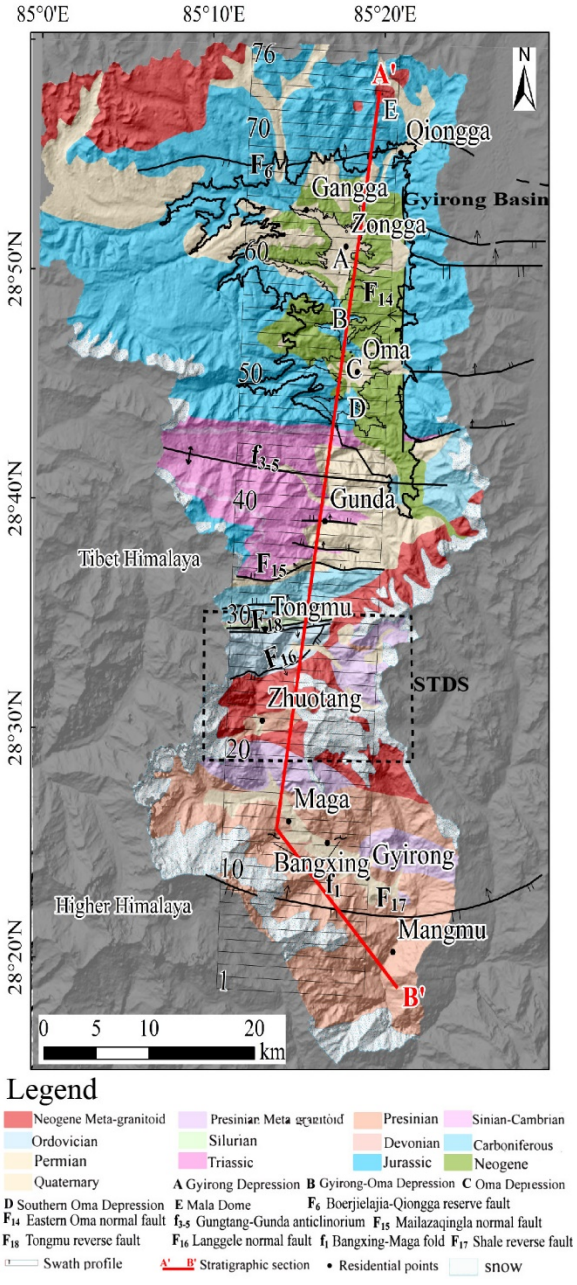

Figure 2. Geological setting of the study area

Other scholars later performed a series of

studies on tectonic geology (Wang et al., 2009), palynological paleogeography (Sun et al., 2007), biostratigraphy (Chen, 1982; Zhu et al., 2008), paleomagnetic chronology (Yue et al., 2004), and so on. They expanded the body of knowledge about the geological evolution and uplift of Himalayan orogen, which has laid a solid research foundation for carrying out digital terrain analysis.

3. MATERIALS AND METHODS

3.1 Data sources and processing

ASTER GDEM and SRTM are two common remote sensing datasets. Because GDEM is derived from the Terra satellite optical sensor while SRTM is from the STS Endeavour OV-105 radar carrier, the latter is qualitatively considered to be more reliable with respect to surface cover interference (Gonga-Saholiariliva et al., 2011). Zhao et al., (2012) and Guo et al., (2011) have compared elevation values from both datasets in forest and city areas with thick surface cover and found varying elevation differences of about 5.42 m-5.31 m; however, they could not prove which DEM was more reliable for terrain index calculation. In fact, both of them contain surface cover height, which can be used to evaluate the natural response of surface cover to terrain variability.

This paper selected an ASTER GDEM 2 for analysis (http://www.gscloud.cn; planar datum: WGS 1984; elevation datum: EGM 96; overall precision with a confidence level of 95%: about 17m; horizontal resolution: about 75m). A geological map of Gyirong County (1:250 000, China Geological Survey, 2003) and vector geographic element data for Chomolungma National Nature Reserve (1:250 000) were also selected, in the same projection as the ASTGTM file.

3.2. Methods

3.2.1. *Swath elevation profile*

To plot a swath elevation profile, a strip of a given width was first identified along cross-sections perpendicular to the main structure of the orogen and then divided into equal interval segments. Then the elevation attribute values for each segment were calculated. Finally, an elevation profile was plotted using segment number as the x-axis and elevation as the y-axis. This type of plot has been extensively applied in orogen scale studies (Burbank, 1992; Frank, 1984; Fielding et al., 1994; Ahmad, 2017). Frank (1984) has shown that there is a nonlinear relationship between the horizontal width scale and elevation range: as horizontal width gradually increases from 10 km to 30 km, the elevation range tends to converge to a constant. According to the area and shape of Gyirong Valley, a 14 km wide and 76 km long swath was divided into 1 km-interval segments, which created 76 14×1 km^2 zones and made up about 50.5% of the total study area. In this way, random elevation sampling was guaranteed and the swath area requirement was satisfied (Fig. 2). Partitioning statistics in ArcGIS were used to calculate the maximum (H_{max}), minimum (H_{min}), and mean elevations ($\bar{H}$), along with elevation ranges (R) for each segment, and MATLAB profile maps were also produced (Fig. 3, based on the raw data in the Table 1 of appendix).

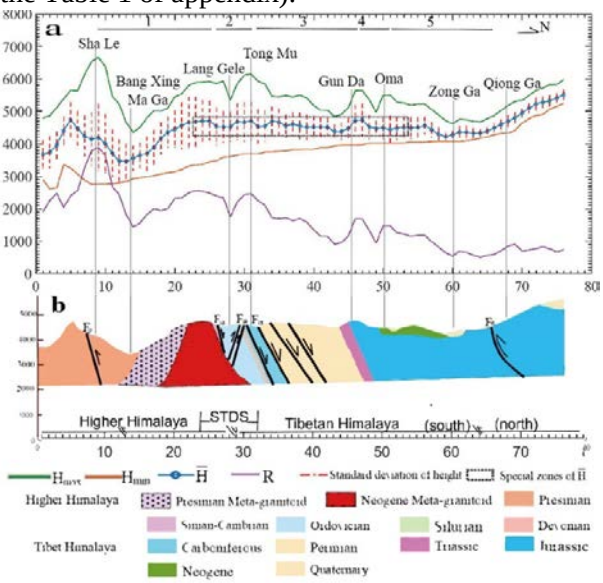

Figure 3. 14×76 km swatch profile of elevations. (a) curves of H_{max}, H_{min}, $\bar{H}$, R and standard deviation of height. (b) stratigraphic section of A'B' in figure 2

Table 1 Raw data of 14*76km swath elevation (m)

ID	H_{max}	H_{min}	$\bar{H}\pm SD$	R
1	4791	2894	3666.97±430.95	1897
2	4864	2612	3733.49±486.04	2252
3	5115	2644	3953.59±409.54	2471
4	5388	3352	4401.79±423.64	2036
5	5644	3250	4740.40±523.80	2394
6	5627	3070	4467.93±514.68	2557
7	6129	2877	4240.54±618.65	3252
8	6534	2755	4141.98±816.79	3779
9	6651	2762	4191.88±1023.02	3889
10	6391	2762	4007.99 ±891.77	3629
11	5460	2778	3702.47±722.70	2682
12	5219	2793	3463.52±658.80	2426
13	4653	2833	3454.63±534.65	1820
14	4359	2922	3557.94±378.56	1437
15	4503	2945	3644.00±381.76	1558
16	4808	2983	3694.58±519.76	1825
17	5011	3019	3891.28±521.88	1992

18	5009	3073	4168.99±484.17	1936
19	5101	3105	4357.27±469.74	1996
20	5449	3137	4452.76±559.89	2312
21	5542	3207	4553.40±707.99	2335
22	5794	3310	4660.79±772.19	2484
23	5892	3333	4680.22±755.21	2559
24	5901	3369	4703.85±624.99	2532
25	5920	3442	4711.16±597.74	2478
26	5864	3476	4535.36±571.32	2388
27	5932	3591	4511.40±474.02	2341
28	5351	3604	4524.81±446.32	1747
29	5851	3648	4681.15±555.95	2203
30	6114	3683	4664.44±599.72	2431
31	6141	3683	4705.55±569.24	2458
32	5931	3683	4527.60±517.58	2248
33	5840	3745	4544.12±461.85	2095
34	5467	3745	4699.00±430.49	1722
35	5451	3764	4663.80±402.41	1687
36	5491	3773	4546.08±341.53	1718
37	5443	3818	4604.84±352.02	1625
38	5507	3818	4548.14±389.92	1689
39	5410	3828	4511.23±377.57	1582
40	5182	3829	4514.96±328.23	1353
41	5029	3882	4517.35±289.33	1147
42	5025	3882	4507.46±268.58	1143
43	4842	3939	4379.78±194.27	903
44	4902	3952	4380.04±257.95	950
45	5110	3952	4480.95±296.12	1158
46	5634	3952	4717.28±469.50	1682
47	5641	3961	4739.27±483.73	1680
48	5366	4032	4511.93±367.35	1334
49	4964	4032	4466.23±229.74	932
50	5500	4032	4482.65±328.54	1468
51	5511	4032	4439.37±408.11	1479
52	5280	4032	4479.65±340.41	1248
53	5255	4032	4510.72±325.95	1223
54	5191	4048	4484.00±325.19	1143
55	5226	4048	4503.30±306.44	1178
56	5226	4048	4557.77±257.99	1178
57	5051	4068	4432.20±221.62	983
58	4886	4073	4298.65±183.59	813
59	4716	4073	4220.49±110.76	643
60	4617	4073	4275.69±103.30	544
61	4756	4073	4362.02±171.94	683
62	4746	4094	4361.57±187.55	652
63	4691	4125	4320.12±145.29	566
64	4672	4169	4330.87±104.21	503
65	4774	4213	4390.06±88.92	561
66	4868	4278	4491.38±133.92	590
67	5023	4319	4599.38±147.72	704
68	5181	4337	4697.78±179.30	844
69	5304	4406	4802.91±154.70	898
70	5333	4634	4943.74±119.97	699
71	5493	4771	5092.93±137.62	722
72	5637	4876	5223.34±185.51	761
73	5719	4897	5276.55±166.63	822
74	5819	5058	5321.19±162.87	761
75	5823	5152	5414.25±129.98	671
76	5976	5244	5515.21±141.18	732

3.2.2 *Relief amplitude*

The key to calculating local relief lies in defining the optimum statistical window (Zhou & Liu, 2006). Adopting the area-elevation difference knee algorithm, Tu & Liu (1990) pointed out that topographic maps with a scale greater than 1:250 000 should preferentially introduce a statistical unit of 2km^2. The quality of an ASTER GDEM with a resolution of 30m is comparable to that of a 1:50 000 topographic maps with a scale greater than 1:250 000 should preferentially introduce a statistical unit of 2km^2. The quality of an ASTER GDEM with a resolution of 30m is comparable to that of a 1:50 000 topographic map (Zhang et al., 2012), so the statistical window can be further narrowed. According to calculations for this study, the projected minimum sub-watershed area was about 1km^2. To prevent an excessively small statistical window from over-smoothing the elevation difference in these sub-watersheds, this paper used 35×35 pixels (1.1 km^2) as the optimum statistical window.

3.2.3 *Average slope*

A statistical window for average slope consistent with relief was needed. The deterministic 8 (D8) method (O'Callaghan & Mark, 1984) was used to calculate the slope angle on the minimum grid (30×30m2) and then a 35×35 window was used to calculate the average slope in ArcGIS zonal statistics.

3.2.4 *Stream network*

The hydrological analysis function in ArcGIS was used to extract the Gyirong watershed river network and calculate river path length and network density (Table 2).

Table 2. Characteristic statistics of the surface runoff vertical differentiation

Elevation(m)	≤4000	4000-5600	≥5600
Area(km2)	333.74	1730.87	153.13
River length (m)	395421.63	1251152.87	8513.98
Density(m/km)	1184.81	722.85	55.60

4. RESULTS

4.1 Swath Elevation Profile

Figures 1 and 2 show that the higher Himalayan crystalline rock zone was mostly covered by 1-25 km segments, while the Tibetan Himalayan Tethyan depositional fold-and-thrust zone was mostly covered by the > 25km segments. The 20 -30 km segments made up the shear zone of the southern Tibetan

detachment system (STDS) (Yang et al., 2009; Zhang et al., 2006). Taking 8-9 km as the boundary (located at the contact surface of the Shaler reverse fault, F_{17} in Fig. 2), the high Himalaya was divided into footwall and hanging walls (Figs 2 and 3b). At the footwall, the summit level (1-8km in Fig. 3a, H_{max}) increased quickly and reached a local maximum (6 651 m) on the F_{17} contact surface. On the other hand, the valley bottom (1-8 km in Fig. 3a, H_{min}) gradually declined and reached a local minimum (2 755 m) on the same surface. This made up the maximum elevation range segment for the whole study area. On the hanging wall, the summit level (9-24 km in Fig. 3a, H_{max}, period 1) had a fluctuating pattern with wide wavelength and deep amplitude. The 13-16 km segments corresponded to the Bangxing-Maga pre-Sinian gneissosity fold structure (Fig.2, f_1) with clear bends in the hillside. On the contrary, the valley bottom (9-24km in Fig. 3a, H_{min}, period 1) features increased very little with no fluctuation or deformation, resulting in the clear variability in elevation range compared with the summit level (Fig.3a).

The Tibetan Himalaya is bounded by the Boerjielajia-Qiongga reverse fault (Fig. 2 F_6 and Fig. 3b) and consists of south and north zones. The tectonic basements of the south zone are the STDS, the eastern fold of Gungthang-Gunda anticlinorium (Fig. 2 $f_{3\text{-}5}$), and the well-known Gyirong Basin (Fig. 2 A-D). The most important tectosome of the north zone is the Mala Dome (Fig. 2 E). The 67-69 km segments were located on the contact surface of F_6, which also served as boundary for elevation variability and there were very different spatial features between the two zones: H_{max} and H_{min} had almost completely different variability. In the south zone (25-67 km in Fig. 3a) along a horizontal extension of about 43km, H_{max} had a four-period fluctuation pattern with a narrow-wide alternating wavelength and shallow-deep alternating amplitude (periods 2-5 in Fig. 3a), while elevations between periods 2-3 and 4-5 exhibited a periodic spatial distribution. In contrast, H_{min} rose continuously 895m at a rate of 21m/km. In the north zone (69 -76 km in Fig. 3), H_{max} and H_{min} increased in a nearly consistent manner. The different spatial features of H_{max} and H_{min} between the two zones also affected elevation range variability (R). In the south zone from 25km to 69km, R was consistent with H_{max}. It is possible that the increase of the valley bottom was too slow to significantly affect the value. In the north zone from 69km on, R no longer increased with H_{max} and only small fluctuations (151m) appeared, suggesting that the summit level was no longer steep and the valley bottom was high enough to leave little space for change.

4.2 Local relief and average slope

For the convenience of observing and comparing terrain features, this paper used a calculation method that was applied in the east-west strike fold-and-thrust belt of the Swiss Alps by Kühni & Pfiffner (2001). It adopted a 200 m contour interval to statistically evaluate relief and average slope for each elevation belt, then plotted the quantitative relationships between relief, slope, and elevation (Figs. 4 and 5, based on the raw data in the tables 3 and 4, respectively).

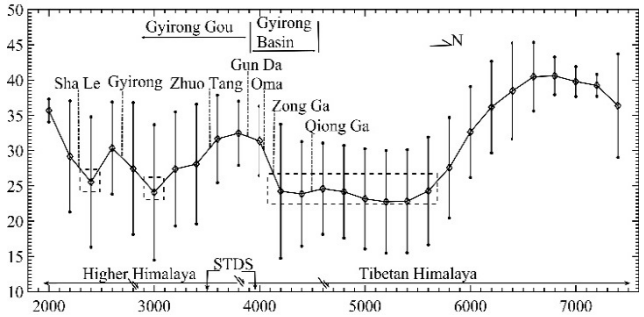

Figure 4. Profile of relief amplitude on 200m elevation interval. There are 3 low relief intervals from 2000 m to 5600 m (dotted rectangle). Vertical solid line is the standard deviation of relief in each elevation interval.

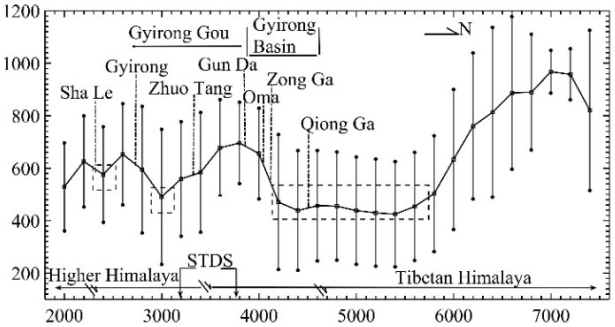

Figure 5. Profile of mean slope on 200m elevation interval. As figure 4, there are 3 slope threshold(~25°) intervals from 2000 m to 5600 m (dotted rectangle). Vertical solid line is the standard deviation of average slope in each elevation interval.

Table 3. Statistic data of relief in 200m interval (m)

ID	Interval	Relief ± SD
1	1800-2000	528.56±167.64
2	2000-2200	625.62±173.34
3	2200-2400	575.59±182.17
4	2400-2600	652.87±193.08
5	2600-2800	594.36±241.17
6	2800-3000	490.37±257.64
7	3000-3200	558.94±218.42
8	3200-3400	583.60±228.17
9	3400-3600	677.39±183.55
10	3600-3800	695.86±154.72
11	3800-4000	655.12±173.07
12	4000-4200	470.39±257.10

13	4200-4400	438.57±228.05
14	4400-4600	456.86±210.31
15	4600-4800	455.26±206.54
16	4800-5000	438.14±204.36
17	5000-5200	429.67±204.02
18	5200-5400	424.58±200.81
19	5400-5600	453.76±205.68
20	5600-5800	502.69±220.75
21	5800-6000	633.18±266.38
22	6000-6200	760.14±278.17
23	6200-6400	812.95±322.93
24	6400-6600	886.37±290.76
25	6600-6800	889.47±220.54
26	6800-7000	967.43±81.64
27	7000-7200	957.46±97.26
28	7200-7400	819.99±305.09

Table 4 statistic data of mean slope on 200m elevation interval

ID	Interval (m)	Mean slop ± SD (°)
1	1800-2000	35.67±1.63
2	2000-2200	29.16±7.87
3	2200-2400	25.53±9.25
4	2400-2600	30.35±6.53
5	2600-2800	27.43±9.34
6	2800-3000	24.07±9.59
7	3000-3200	27.38±8.09
8	3200-3400	28.08±8.50
9	3400-3600	31.65±6.20
10	3600-3800	32.47±4.53
11	3800-4000	31.36±4.91
12	4000-4200	24.23±9.51
13	4200-4400	23.85±7.42
14	4400-4600	24.59±6.47
15	4600-4800	24.15±6.57
16	4800-5000	23.15±7.10
17	5000-5200	22.73±7.27
18	5200-5400	22.81±7.31
19	5400-5600	24.26±7.63
20	5600-5800	27.56±7.12
21	5800-6000	32.62±6.43
22	6000-6200	36.15±6.51
23	6200-6400	38.45±6.79
24	6400-6600	40.47±4.88
25	6600-6800	40.58±2.66
26	6800-7000	39.78±2.11
27	7000-7200	39.23±1.55
28	7200-7400	36.37±7.33

The relief and average slope of the study area were differentiated in the vertical direction, as indicated by the following aspects: i) during the increase in elevation from 2000 m to 4000 m, ground fluctuations and mean slope were relatively steep, but significantly reductions were observed at two other elevation intervals (2200-2400 m and 2800-3000 m) (Figs. 4 and 5). A contour view of 2000-4000 m showed that the slope width gradually decreased northward along the Gyirong River (Fig. 6). ii) the region from 4000 m to 5600 m had an area of 1 730.87 km^2 and accounted for 82.08% of the total area (Table 2). Broad hillsides represented the least fluctuation and mean slope in the whole study area (Figs. 4 and 5), however; and iii) at elevations ＞5600m, hillsides were already close to the periglacial region and occupied an area of only 153.13 km^2 (Table 2 and Fig. 6).

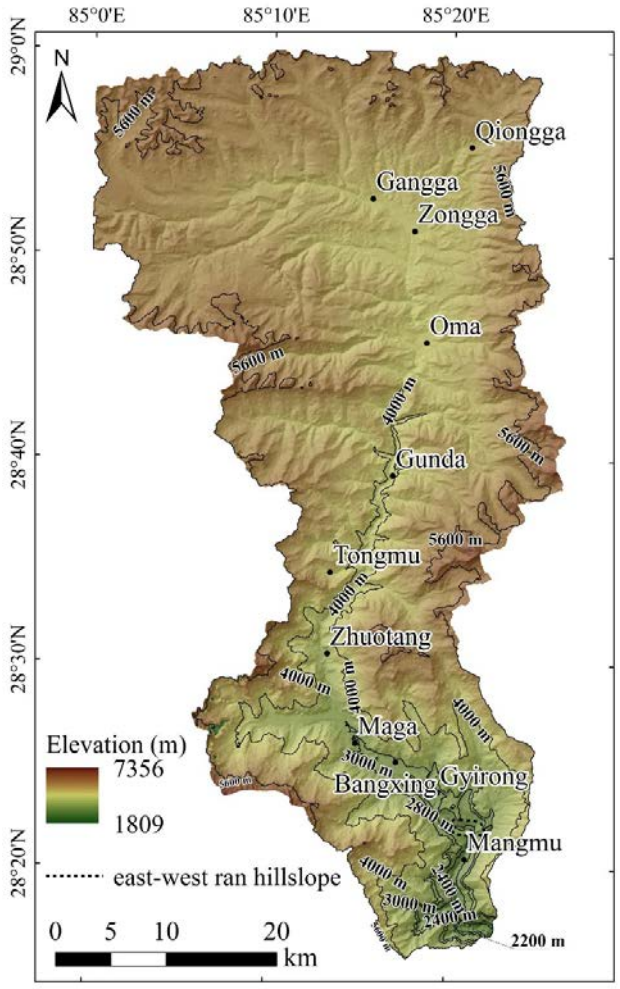

Figure 6. The spatial differentiation and digital terrain of study area

Dramatic increases in relief and slope indicated that the topography was different from other elevation intervals, however. Table.1 shows that the river network length at 4000-5600m elevation was twice the length at elevations of ≤4 000m; river network density of the former was only 61% of that of the latter, however. The spatial distribution of surface erosion in the Gyirong watershed was also very significant.

5. DISCUSSION

5.1 Elevation response to tectonic basements

Comparing Figs 2 and 3, it can be seen that

H_{max} had a regular response to fault and fold distribution. This regularity was manifested by summit level uplift in the reverse faults and anticline, and a decline with the normal faults and folds. To be specific, there were four uniform uplifted summit levels: the 8km segment (Shale reverse fault, F_{17}), the 30km segment (two reverse faults in Tongmu Village, F_{18}), the 46km segment (the north limb of the Gungthang-Gunda anticlinorium ($f_{3\text{-}5}$) that may have concealed reverse faults), and the 67-69km segment (the Boerjielajia-Qiongga reverse fault (F_{16})). In the other segments, the 14km band was a pre-Sinian gneissosity fold (f_1), the 28km band was Langgele normal fault (F_{16}), and the 32-43km band consisted of Mailazaqingla four secondary normal faults (F_{15}) with uniformly decreasing summit levels.

Wang (2008) proposed that Gyirong Basin basements were composed of a tilted fault block caused by listric normal faults. Based on comparisons of summit morphology, this paper speculated that it might be a normal and thrust combined structure. Figure 3 shows the summit level first narrowed and then widened during periods 4-5, which was extremely similar to periods 2-3 in length and width. Periods 2-3 corresponded to the Langgele normal fault (F_{16}), Tongmu reverse faults (F_{18}), and Mailazaqingla normal faults (F_{15}). There may have been a corresponding normal/reverse fault structure in the Gyirong Basin basement during periods 4-5. Additional indirect evidence was on the eastern side of the Eastern Oma normal fault (F_{14}), where two sets of east-west parallel high-angle normal faults developed in each band at latitudes roughly corresponding to the north and south boundaries of the southern Oma Depression (47km band and 51km band in Fig. 2). Two more sets of east-west parallel high-angle reverse faults developed at latitudes roughly corresponding to the county and Gangga Village of northwest Gyirong County (60km band and 64km band in Fig. 2). F_{14} emerged from the east-west stretching tectonics of the Qinghai-Tibet Plateau in the late Miocene (Zhang, 2007; Garzione et al., 2003), cutting off the Triassic and Jurassic strata originally distributed continuously along the east-west tectonic direction, and formed the eastern boundary of the Gyirong Basin. After entering the Quaternary, the faults resumed activity, which may have continued until modern times. Seismic evidence has also shown that F_{14} may have extended its influence as far as Gyironggou (Jr. Hurtado et al., 2001) and that its active tectonics passed through the orogenic ridge. In this case, it may have given rise to the tilt and deformation of previously concealed faults, which would have combined with the basement of a normal/reverse fault.

5.2 Average elevation variability and indications of Himalayan uplift and erosion

With an elevation of 4000m as the rough boundary, the average elevation($\bar{H}$) first increased (< 4000m) and then stabilized (> 4000 m). This reflected the equilibrium influence on hillside height under uplift-denudation and sedimentation processes. In the higher Himalaya it was consistent with fluctuations in H_{max} and R (1-20 km in Fig.3a). In the STDS and most of the Tibetan Himalaya（20-56km in Fig. 3a), however, a clear relative equilibrium height of about 4560 m was maintained. On the other hand, the standard deviation increased with increasing summit height and decreased with decreasing summit height in the same interval, thus ensuring the stability of $\bar{H}$. (Adams et al., 2016), applied a 30 km horizontal width swath to calculate the terrain index in the eastern Himalayan hinterland in Bhutan, 89°-91°30′E and 27°-28°N, pointing out that within the average elevation region of 3000 m - 3500 m, there were four groups of parallel low and small scale geomorphic units (<200 m), which were explored to the high altitude alluvial basins under Himalayan glacial rivers. These basins have important relationships with the long-term effects of Himalayan uplift subsidence - denudation sedimentation processes. In this paper, the 14×76km strip was located west of Adams (2016) study area (85°E) with basically the same latitude (28°30′-28°50′N), and the $\bar{H}$ of the 20-56km segments also had high-elevation and low-relief characteristics, which developed at the bottom of the alluvial basin in the upper reaches of the Gyirong River. To a degree, this can reflect to the tectonic characteristics of middle Himalayan orogen.

Li et al., (2015) and Li et al., (1979) proposed that during the C phase of “the Qinghai-Tibet movement” (2.0-1.7Ma), the Himalayas uplifted strongly and rapidly. During the Kunlun-Yellow River movement (1.2-0.6Ma), most mountains were pushed into the cryosphere at 0.8Ma (Wang et al., 1996), and reached 4,000-4,500m (Li & Fang, 1998). Around 1.7Ma the Gyirong Basin was captured by the southern water system and the enclosed lacustrine basin turned into an outward river channel accompanied by strong river erosion. Around the middle Pleistocene (~0.8Ma) glacial erosion joined the geomorphological shaping process, and from the end of the middle Pleistocene glaciation weakened and retreated. The modern river system pattern of the middle Himalayan orogen didn’t take shape until the Holocene (0.13Ma). It can be seen that the rapid uplift of the Gyirong watershed to its modern elevation and large-scale

erosion sedimentation was mostly completed during the Pleistocene period, with a duration of about 1.5Ma. In this very short geological period, it was impossible to complete the process of heightening and filling the Himalayas, but local accumulation or alluvial landforms may have developed.

5.3 Relationship between relief, average slope, and stable hillsides

Local relief and mean slope can describe hillside variability in the vertical direction, but to interpret these features it is necessary to consider the dynamic mechanisms of denudation and sedimentation. Schmidt & Montgomery (1995), in their study of plutonic bedrock landslide bodies in the Cascade Range and Santa Cruz Mountains of North America, adopted the maximum stable hillslope model to calculate the cohesive stress and frictional angle of slope materials and confirmed that material strength, tectonics, and climate influenced the fluctuation limits of mountains. similarly, Kühni & Pfiffner (2001) argued that erosion constantly altered slope size, creating relative slope stability by gradually reducing the slope angle, and obtained a mean slope angle threshold of 25° on a mean slope profile of the fold-and-thrust belt of the Swiss Alps' Jura Mountains.

As shown in figure 4, hillsides with a slope angle near 25° were distributed along three height belts, beginning at the lowest: 1) from 2200-2400 m, with 25.53° mean slope and 575.6 m local relief, Precambrian metamorphic rocks were observed. The hillside was expanding on the F_{17} footwall, where the northern end pulled the block in the fault contact surface zone transition facing WE by about 2km (Fig. 6); 2) from 2800-3000 m, with 24.07° mean slope and 490.4m local relief, this belt was mainly distributed along the Gyring River through Maga-Bangxing-Gyirong Town. Zhu (1995) has pointed out that glacial erosion landforms were significant in the region; and 3) the elevation interval of 4 000m-5 600m had a mean slope of 22.73°-24.59° with consistently steady variability in local relief (Fig. 4). Furthermore, the hillside mostly overlapped with the 20-56 km swath in figure 2. Compared with the mountains studied by Kühni & Pfiffner (2001) and Schmidt &Montgomery (1995), the Gyirong watershed was a stable hillside with a slope threshold near 25° (i.e. 2000 m, 3000 m, 4000 m, Fig. 5), elevation of 2000-3000 m higher, and a small-scale landform. The results showed that while different orogens had significant spatial differences with respect to climate conditions, geomorphological types, tectonics, and strata, erosion was probably still the driving force behind equilibrium for heterogeneous hillsides at different scales.

6. CONCLUSIONS

This paper conducted digital topographic analysis in a small-scale region at very high altitudes in the Himalayan Mountains. Taking full advantage of Aster GDEM2 data, three basic topographic indices were calculated to obtain tectonic characteristics in the Gyirong watershed and evaluate change in Himalayan uplift and erosion at the basin scale, while comparing the effectiveness of mean slope angle threshold between different orogens and the inner Gyirong. This information can be used for reference and reveals the internal relationship between digital topographic indexes and the development of orogenic belts.

The topographic elevation characteristics corresponded to local basement forms and tectonic associations. The spatial periodic change in H_{max} responded to the structural distribution. This was first manifested in the uplift of the summit in reverse faults and anticlines, and in the decline of the summit with normal faults and folds. The jagged summit probably also supported combined normal/reverse faults in the basement of Gyirong Basin. Average height increased rapidly in STDS and then stabilized at the center of the Tibetan Himalaya, where 4000m was the vertical differentiation boundary of tectonic landforms. Comparing the hillside features of Swiss Alps and the Gyirong watershed, although the climate, landforms, tectonics, and lithology were different across different orogenic belts, erosion was the tectonic genesis of equilibrium for heterogeneous hillsides at different scales.

Acknowledgements

This work was financially supported by the NNSF C1461029 and the PTI YJRC2016-6. We thank Director Qimi Ciren, the energy research and demonstration center, TAR for the NSFTAR XZ2017ZRG-99 Grant help. We also thank the support of Ir. Jun He for useful information of the study area. The NNSFC 41161067 and NSFTAR 2015ZR-13-66 provided the necessary research materials.

REFERENCES

Adams, B. A., Whipple, K. X., Hodges, K. V. & Heimsath, A. M., 2016. *In situ development of high-elevation, low-relief landscapes via duplex deformation in the Eastern Himalayan hinterland, Bhutan*. Journal of Geophysical Research: Earth

Surface, 121, 2, 294-319.

Ahmad, S., 2017. *Impact of climate-tectonic interaction on terrain characteristics of the watersheds in western Himalaya.* Carpathian Journal of Earth and Environmental Sciences, 12, 1, 13-21.

Artugyan, L. & Urdea, P., 2016. *Using digital elevation model (DEM) in karst terrain analysis. Study case: Anina mining area (Banat Mountains, Romania).* Carpathian Journal of Earth and Environmental Sciences, 11, 1, 55-64.

Burbank, W. D., 1992. *Characteristic size of relief.* Nature, 359, 483-484.

Chen, L., Ma, F., Qin, J. X. & Kan, A. K., 2011. *Spatial Distribution characteristics of Land use in the Mid. Himalaya Mountain Area.* Resources Science, 33, 8, 1584-1590.

Chen, W. Y., 1982. *Pliocene Environment of Hipparion Fauna of Middle Himalaya Range.* Vertebrata Palasiatica, 20, 1, 45-54. (In Chinese)

Dong, S. P., Zhang, P. Z., Zhang, H. P., Wen, J. Z. & Chen, H. X., 2018. *Drainage responses to the activity of the Langshan Range-Front Fault and tectonic implication.* Journal of Earth Science, 29, 1, 193-209.

Fielding, E., Isacks, B., Barazangi, M., Barazangi. M. & Duncan. C., 1994. *How flat is Tibet?* Geology, 22, 163-167.

Frank, A., 1984. *Local relief and the height limits of mountain ranges.* American Journal of Science, 284, 9, 1035-1055.

Garzione, C. N., DeCelles, P., Hodkinson, D. G., Ojha, T. P. & Upreti, B. N., 2003. *East-west Extension and Miocene Environmental Change in the Southern Tibetan Plateau: Thakkholagraben, Central Nepal.* Geological Society of American Bulletin, 115, 1, 3-20.

Gonga-Saholiariliva, N., Gunnell, Y., Harbor, D. & Meringe, C., 2011. *An automated method for producing synoptic regional maps of river gradient variation: Procedure, accuracy tests, and comparison with other knickpoint mapping methods.* Geomorphology, 134, 3-4, 394-407.

Gonga-Saholiariliva, N., Gunnell, Y. & Petit, C., 2013. *Techniques for quantifying the accuracy of gridded elevation models and for mapping uncertainty in digital terrain analysis.* Progress in Physical Geography, 35, 6, 739-764.

Guo, X. Y., Zhang, H. Y., Zhang, Z. X., HOU, G. l. & ZHAO, J. J., 2011. *Comparative Analysis of the Quality and Acduracy between ASTER-GDEM and SRTM3.* Remote Sensing Technology and Application, 26, 3, 334-339.

Jr. Hurtado, J. M., Hodges, K. V. & Whipple, K. X., 2001. *Neotectonics of the Thakkhola graben and Implications for Recent activity on the South Tibetan Fault System in the Central Nepal Himalaya.* Geological Society of America BUlletin, 113, 2, 222-240.

Kühni, A. & Pfiffner, O. A., 2001. *The relief of the Swiss Alps and adjacent areas and its relation to lithology and structure: topographic analysis from a 250-m DEM.* Geomorphology, 41, 4, 285-307.

Le Fort, P., 1996. *Evolution of the Himalaya*. - In: **Yin, An; Harrison, T M**, *The Tectonics of Asia*. Cambridge University Press, New York. 95-106.

Li, J. J., Wen, S. X., Zhang, Q. S., Wang F. B., Zhen, B. X. & Li. B. Y., 1979. *Discussion on the Times, ranges and forms of the uplift of the Qinghai-Tibet Plateau.* Science China, 6, 608-616.

Li, J. J. & Fang, X. M., 1998. *Study on uplift and environmental change of Qinghai-Tibet Plateau.* Chinese Science Bulletin, 43, 15, 1569-1574.

Li, J. J., Zhou, S. Z., Zhao, Z. J. & Zhang. J., 2015. *The Qingzang Movement: The Major Uplift of The Qinghai-Tibetan Plateau.* Science China: Earth Sciences, 45, 10, 1597-1608.

Molnar, P. & Tapponnier, P., 1975. *Cenozoic Tectonics of Asia: Effects of a Continental Collision.* Science, 189, 419-426.

O'Callaghan, J. F. & Mark, D. M., 1984. *The extraction of drainage networks from digital elevation data.* Computer Vision, Graphics, and Image Processing, 28, 323-344.

Petrik, A. & Jordan, G., 2017. *Systematic digital terrain model construction and model verification with multi-source field data. Morphotectonic analysis in the Villany Hills and its surroundings, SW Hungary*. Carpathian Journal of Earth and Environmental Sciences, 12, 1, 207-224.

Schmidt, K. M. & Montgomery, D. R., 1995. *Limits to Relief.* Science, 270, 5236, 617-620.

Sun, L. M., Yan, T. S., Tang, G. Y.， Ding, X. Y., Wang, R. J. & Tian, L. F., 2007. *Neogene Sporopollen Assem Blages and Paleogeography in the Gyirong Basin, Tibet.* Geology in China, 34, 1, 49-54.

Tu, H. M. & Liu, Z. D., 1990. *Demonstrating on Optimum Statistic Unit of Relief Amplitued in China*. Journal of Hubei University (Natural Science), 12, 3, 266-271.

Vijith, H., Prasannakumar, V., Sharath Mohan, M. A., Ninu Krishnan, M. V. & Pratheesh, P., 2017. *River and basin morphometric indexes to detect tectonic activity: a case study of selected river basins in the South Indian Granulite Terrain (SIGT).* Physical Geography, 38, 4, 360-378.

Wang, D. C., 2008. *Tectonic and Environmental Evolution of the Gyirong Basin, and its Relationship to the uplift of Tibetan Plateau.*M.D. thesis, Peking University,11.

Wang, D. C., Zhang, J. J., Yang, X. Y. & Qi, G. W., 2009. *Tectonic and Environmental Evolution of Gyirong Basin, and its Relationship to the Uplift of Tibetan Plateau.* Acta Scientiarum Naturalium Universitatis Pekinensis, 45, 1, 79-89.

Wang, F. B., Li, S. F., Shen, X. H., Zhang. J. & Yan. G., 1996. the Formation and Evolution, Environmental Transition of Gyirong *Basin and uplift of Himalaya.* Science in China (Series D), 26, 4, 329-335.

Xu, J. X., Li, B. Y., Yang, X. P., Zhou, L. P., Shi, C. X., Gao, S., Zheng, X .M., Xiong, K .N., Zhu, B. Q., Wang, Y .P. & Zhou, L. M., 2009. *Recent Progress in Geomorphology and Quaternary Geology in China and Some Perspectives.* Acta Geographica Sinica, 64, 11, 1375-1393.

Yang, X. Y., Zhang, J. J., Qi, G. W., Wang, D. C., Guo, L., Li, P. Y. & Liu, J., 2009. *Structure and deformation around the Gyirong basin, northern Himalaya, and onset of the south Tibetan detachment system.* Sci China Ser D-Earth Sci,52, 8, 1046-1058.

Yin, A., 2006. *Cenozoic Tectomic Evolution of the Himalayan Orogen as Constrained by Along-strike Variation of Structural Geometry, Exhumation History, and Foreland Sedimentation.* Earth Science Frontiers, 13, 5, 416-515.

Yue, L. P., Deng, T., Zhang, R., Zhang, Z. K., Heller, F., Wang, J. Q. & Yang, L. R., 2004. *Paleomagnetic Chronology and Records of Himalayan Uplift on the Longgugou Section of Gyirong-Oma Basin the Xizang (Tibet).* Chinese Journal of Geophysics, 47, 6, 1009-1016.

Zhang, Z. L., Sun, X., Li, G. D., Zhang, J. D., Liu, H. Z., Zhuan, S. P. & Wei, W. T., 2006. *New explanation of detachment structures in the Burang and Gyironggou regions, southern Xizang.* Sedimentary Geology and Tethyan Geology, 26, 2, 1-6.

Zhang, J. J., 2007. *A Review on the Extensional Structures in the Northern Himalaya and Southern Tibet.* Geological Bulltin of China, 26, 6, 639-649.

Zhang, C. M., Liu, Q. S., Liu, G. H., Ding, S. W., Wang, P. & Dong, J. F., 2012. *Data Processing and Application Progress of SRTM 3 and ASTER GDEM.* Geography and Geo-Information Science, 28, 5, 29-34.

Zhao, G. S., Du, Y., Ling, F. & Li, X. D., 2012. *Analysis of Influencing Factors on Height Differences between ASTER GDEM and SRTM3.* Science of Surveying and Mapping, 37, 4, 167-170.

Zhou, Q. M. & Liu, X. J., 2006, *Digital terrain analysis*. China Science Publishing, Bei Jing. 112.

Zhu, C., 1995. *Neotctonism and Quaternary Glaciation of Gyirong Basin, Xizang.* Mountain Research, 13, 4, 219-225.

Zhu, C. F., Tian, L. F., Sun, L. M. & Zhang, Z. L., 2008. *Permian Biostratigraphy from the Jilong Area, Southern Xizang.* Journal of Stratigraphy, 32, 3, 333-339

Received at: 13. 02. 2019
Revised at: 17. 07. 2019
Accepted for publication at: 21. 07. 2019
Published online at: 24. 07. 2019